

Cole S. Stapleton, Christopher J. Shaffer, Dana R. Reed

Cole S. Stapleton, Christopher J. Shaffer, Dana R. Reed

Algorithm Improvements

Results and Conclusion



With incredible resolution, sensitivity, and peak capacity available for LC/MS, experiments can often contain 100-1000's of potential compounds, also known as features. Identification of these features can be challenging with these large sample species are often present as either the compounds of interest or some kind of background, due to plastic contamination. Thus, almost any unknowns' analysis can benefit from these improvements.



Origins of Kendrick Mass Defect

Kendrick Mass Defect (KMD) analysis originated from petroleomics to classify hydrocarbon saturated petroleum reserves containing CH_2 repeats. KMD hinges upon the change from ^{12}C to ^{13}C to a new mass basis for example CH_2 14.0014 \rightarrow 14.0000. This been applied and improved upon for several decades with the utilization of fractional Kendrick Mass Defect (1), shift factors (seen in some software packages), and further extensions of KMD to classify polymers (5, 8). The algorithms used in KMD transform values from the mass or m/z domain to a new KMD domain. Typically, this includes a change in mass basis through scaling, followed by decimal or defect analysis. "KMD-like" algorithms are those that broadly follow these steps to determine repeat units within mass spectral data.

1.) *Scale mass axis*1.) *Scale mass axis*

2.) Calculate decimal value or defect

$$KMD = KM - round(KM)$$

$$fMR = \left(m/z * \frac{n}{RI} \right) \% 1, \quad n = 1, 2, 3 \dots$$

$$fMR = \left(m/z * \frac{n}{RI} \right) \% 1, \quad n = 1, 2, 3 \dots$$

Most recent and popular advancements in KMD-like algorithms utilized in polymer analysis include fractional KMD and Mass Remainder Analysis (MARA) (1, 5). To build upon these approaches, we present fractional Mass Remainder (fMR), which is a KMD-like approach. It improves upon previous works which is shown through algorithmic insight based on analysis and error propagation, circular distance metrics for repeat unit determination with data scientific approaches. We highlight previous short-comings, algorithmic improvements and conceptual recapitulation upon KMD-like algorithms through notation and general analysis, error analysis, and data scientific approaches. The applications of this work are further described at poster [THP43](#)

Conflicts of Interest: The authors declare no competing financial interest.

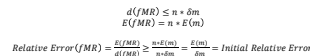
References

1. Fougère, T.; Cabié, B.; Sani, H. (2017) Investigating the Role of Kinetic Mass Defect Analysis for Polymer Loss with Fractional Noise. *Math. Mesoscopy*, **6**, 1. <https://doi.org/10.1007/s00033-017-0955-4>
2. Fougère, T.; Cabié, B.; Sani, H. (2017) Capabilities of the remainder of residual Karhunen modes and the reflected Karhunen modes deficit for copolymer noise. In *Journal of Mathematical Sciences*, **230**, 103–117. <https://doi.org/10.1007/s12220-017-9811-4>
3. Fougère, T.; Cabié, B.; Sani, H. (2018) Evaluation of the Karhunen Mass Defect Analysis for the Randomness in Low Resolution and High Range Maps. *European Physical Journal Special Topics*, **227**, 115–126. <https://doi.org/10.1140/epjst/e2017-06704-4>
4. Korf, A.; Fougère, T.; Schmid, R.; Hoyer, H.; Al-Haghiel, S. (2020) Expanding the Karhunen mode method to higher mass 2 to enable rapid polymer characterization in Rapid Scanning Atomic Force Microscopy. *ACS Applied Materials*, **13**, 1000–1009. <https://doi.org/10.1021/acsami.9b22049>
5. Yagci, Y.; Kaki, A.; Zengin, M.; Kulu, S.; Kucuk, S.; Karadas, A. (2016) A New Data Mining Tool for Polymer Characterization. *Advances in Chemistry*, **980**, 1002–1007. <https://doi.org/10.1002/9781118999999.ch53>
6. Fougère, T.; Cabié, B.; Sani, H. (2018) Karhunen Modes and the Mass Defect Analysis for the Randomness in Low Resolution and High Range Maps. *European Physical Journal Special Topics*, **227**, 115–126. <https://doi.org/10.1140/epjst/e2017-06704-4>
7. Fougère, T.; Cabié, B.; Sani, H. (2018) Karhunen Modes and the Mass Defect Analysis for the Randomness in Low Resolution and High Range Maps. *European Physical Journal Special Topics*, **227**, 115–126. <https://doi.org/10.1140/epjst/e2017-06704-4>
8. Fougère, T.; Cabié, B.; Sani, H. (2018) Karhunen Modes and the Mass Defect Analysis for the Randomness in Low Resolution and High Range Maps. *European Physical Journal Special Topics*, **227**, 115–126. <https://doi.org/10.1140/epjst/e2017-06704-4>
9. Fougère, T.; Cabié, B.; Sani, H. (2018) Karhunen Modes and the Mass Defect Analysis for the Randomness in Low Resolution and High Range Maps. *European Physical Journal Special Topics*, **227**, 115–126. <https://doi.org/10.1140/epjst/e2017-06704-4>
10. Fougère, T.; Cabié, B.; Sani, H. (2018) Karhunen Modes and the Mass Defect Analysis for the Randomness in Low Resolution and High Range Maps. *European Physical Journal Special Topics*, **227**, 115–126. <https://doi.org/10.1140/epjst/e2017-06704-4>
11. Fougère, T.; Cabié, B.; Sani, H. (2018) Karhunen Modes and the Mass Defect Analysis for the Randomness in Low Resolution and High Range Maps. *European Physical Journal Special Topics*, **227**, 115–126. <https://doi.org/10.1140/epjst/e2017-06704-4>
12. Fougère, T.; Cabié, B.; Sani, H. (2018) Karhunen Modes and the Mass Defect Analysis for the Randomness in Low Resolution and High Range Maps. *European Physical Journal Special Topics*, **227**, 115–126. <https://doi.org/10.1140/epjst/e2017-06704-4>
13. Fougère, T.; Cabié, B.; Sani, H. (2018) Karhunen Modes and the Mass Defect Analysis for the Randomness in Low Resolution and High Range Maps. *European Physical Journal Special Topics*, **227**, 115–126. <https://doi.org/10.1140/epjst/e2017-06704-4>
14. Fougère, T.; Cabié, B.; Sani, H. (2018) Karhunen Modes and the Mass Defect Analysis for the Randomness in Low Resolution and High Range Maps. *European Physical Journal Special Topics*, **227**, 115–126. <https://doi.org/10.1140/epjst/e2017-06704-4>
15. Fougère, T.; Cabié, B.; Sani, H. (2018) Karhunen Modes and the Mass Defect Analysis for the Randomness in Low Resolution and High Range Maps. *European Physical Journal Special Topics*, **227**, 115–126. <https://doi.org/10.1140/epjst/e2017-06704-4>
16. Fougère, T.; Cabié, B.; Sani, H. (2018) Karhunen Modes and the Mass Defect Analysis for the Randomness in Low Resolution and High Range Maps. *European Physical Journal Special Topics*, **227**, 115–126. <https://doi.org/10.1140/epjst/e2017-06704-4>
17. Fougère, T.; Cabié, B.; Sani, H. (2018) Karhunen Modes and the Mass Defect Analysis for the Randomness in Low Resolution and High Range Maps. *European Physical Journal Special Topics*, **227**, 115–126. <https://doi.org/10.1140/epjst/e2017-06704-4>
18. Fougère, T.; Cabié, B.; Sani, H. (2018) Karhunen Modes and the Mass Defect Analysis for the Randomness in Low Resolution and High Range Maps. *European Physical Journal Special Topics*, **227**, 115–126. <https://doi.org/10.1140/epjst/e2017-06704-4>
19. Fougère, T.; Cabié, B.; Sani, H. (2018) Karhunen Modes and the Mass Defect Analysis for the Randomness in Low Resolution and High Range Maps. *European Physical Journal Special Topics*, **227**, 115–126. <https://doi.org/10.1140/epjst/e2017-06704-4>
20. Fougère, T.; Cabié, B.; Sani, H. (2018) Karhunen Modes and the Mass Defect Analysis for the Randomness in Low Resolution and High Range Maps. *European Physical Journal Special Topics*, **227**, 115–126. <https://doi.org/10.1140/epjst/e2017-06704-4>
21. Fougère, T.; Cabié, B.; Sani, H. (2018) Karhunen Modes and the Mass Defect Analysis for the Randomness in Low Resolution and High Range Maps. *European Physical Journal Special Topics*, **227**, 115–126. <https://doi.org/10.1140/epjst/e2017-06704-4>
22. Fougère, T.; Cabié, B.; Sani, H. (2018) Karhunen Modes and the Mass Defect Analysis for the Randomness in Low Resolution and High Range Maps. *European Physical Journal Special Topics*, **227**, 115–126. <https://doi.org/10.1140/epjst/e2017-06704-4>
23. Fougère, T.; Cabié, B.; Sani, H. (2018) Karhunen Modes and the Mass Defect Analysis for the Randomness in Low Resolution and High Range Maps. *European Physical Journal Special Topics*, **227**, 115–126. <https://doi.org/10.1140/epjst/e2017-06704-4>
24. Fougère, T.; Cabié, B.; Sani, H. (2018) Karhunen Modes and the Mass Defect Analysis for the Randomness in Low Resolution and High Range Maps. *European Physical Journal Special Topics*, **227**, 115–126. <https://doi.org/10.1140/epjst/e2017-06704-4>
25. Fougère, T.; Cabié, B.; Sani, H. (2018) Karhunen Modes and the Mass Defect Analysis for the Randomness in Low Resolution and High Range Maps. *European Physical Journal Special Topics*, **227**, 115–126. <https://doi.org/10.1140/epjst/e2017-06704-4>
26. Fougère, T.; Cabié, B.; Sani, H. (2018) Karhunen Modes and the Mass Defect Analysis for the Randomness in Low Resolution and High Range Maps. *European Physical Journal Special Topics*, **227**, 115–126. <https://doi.org/10.1140/epjst/e2017-06704-4>
27. Fougère, T.; Cabié, B.; Sani, H. (2018) Karhunen Modes and the Mass Defect Analysis for the Randomness in Low Resolution and High Range Maps. *European Physical Journal Special Topics*, **227**, 115–126. <https://doi.org/10.1140/epjst/e2017-06704-4>
28. Fougère, T.; Cabié, B.; Sani, H. (2018) Karhunen Modes and the Mass Defect Analysis for the Randomness in Low Resolution and High Range Maps. *European Physical Journal Special Topics*, **227**, 115–126. [https://doi.org/10.1140/epjst/e2017-06](https://doi.org/10.1140/epjst/e2017-06704-4)

The notation and discussion introduced here is explicitly implemented within Python but can be extended across any programming language. The use of modulo (%) gives similar intermediary result as the typical notation, except the function is flipped and shifted to a new domain. The final result is not impacted by this because the analysis utilizes the relative difference between measurements. In addition, modulo operators are also inherently circular, inspiring the conceptual diagrams described in section 4.



Through error analysis, no improvement of the mass resolution is given from higher values of the coefficient, X , the coefficients are highlighted above in yellow. When considering any 2 mass measurements, they have a distance, $d(\text{IMR})$, and errors, $E(\text{IMR})$. The relative error defined as the ratio of distance to error, then decreases at some value n in fractional mass remainder. This then limits the ability to discriminate polymeric species.



An inherent redundancy within fractional KMD has been noted previously, observed in the isotope spacing within a given mass spectrum (1). This can be found when using different values for the fractional value, n , as shown through analysis below. The coefficient in the fractional KMD term highlighted depends on the repeat unit and fractional value, n . By requiring this arbitrary value, this leads to excessive manual searching and inefficiency within algorithms. Thus, the proposed improvement is to implement fractional Mass Remainder stemming from the following works.

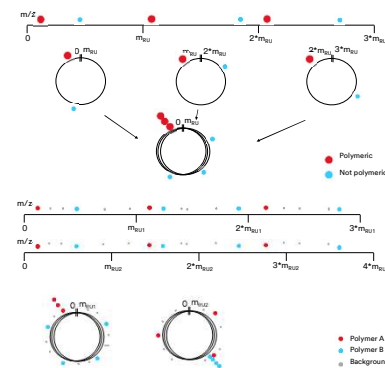
Redundancy Parameter from ρ -Function – Figures contain calculated KMO coefficients (Left) and synthetic data of a polymeric (PDE) species with isotopes ^{13}C and ^{15}N . Separation of the species is identified when $\rho = 1, 2, 4$. Simultaneously, $n = 3$ to 5 also shows the same data separation.

$$X = \frac{\text{KMO}(\text{PDE}) \times 100}{\text{KMO}(\text{PDE}) + 1}$$

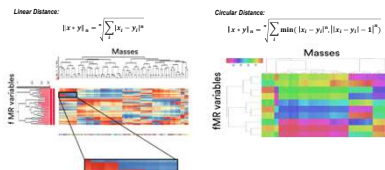
ρ	X
1	50
2	66.66
4	80
5	83.33
6	85.71

Circular distance metrics have been used in other fields (9) but has not been used for KMD-like algorithms, to the best of our knowledge. Distance metrics are a key factor in many types of analysis such as clustering, dimension reduction, and various other data scientific approaches. Selection of the proper distance metric is essential for a given analysis, especially in polymer determination methods.

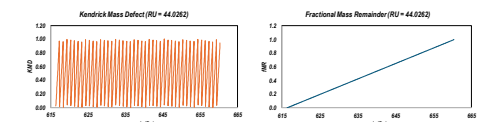
For a given repeat unit (RU), IMR first applies a scaling step which transforms the m/z axis from 0 - RU \rightarrow 0 - 1. Then the scaled m/z axis is segmented at the integer multiples of RU (1, 2, 3, ...). When the circular distance metric is applied, the distance between the end-points of those segments is set equal to 0. This can be represented by mapping the line segments onto circles. Finally, every segment maps onto the sample circle, shown by overlaying each one. It is shown below how evenly spaced masses stack up when this is done for either a single repeat unit (top) or multiple repeat units (bottom).



Due to the inherent discontinuity displayed throughout this work, points can arbitrarily seem far apart on a linear plot and can depend on notation. Masses with a KMD value near ± 0.5 in a traditional KMD approaches can lead to incorrect assignment due to the sampling error of a given group over that cusp, in a linear representation. The figures below show a split cluster near the cusp contain both end-points red and blue (Left) versus a circular distance and color map where clusters containing a single color (Right).

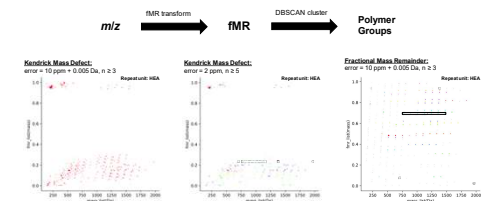


Below the KMD (Left) and IMR (Right) transformations applied to all points on the m/z axis are shown, when the repeat unit is polyethylene glycol (PEG). Both figures span a single repeat unit across the m/z axis. For IMR, by design the number line has distinct values for every given fractional value. KMD on the other hand, stacks 44 values on top of each other in a single given repeat unit, despite not actually being a single PEG unit apart.



Interpretation of any KMD-like algorithm has its challenges when manually visualizing. This can be seen in the figures below. In the case of fMR, scaling and zoom can become a large challenge. When KMD is applied, values overlap and become difficult to interpret. The recommended approach is then to use some type of sort, clustering, or other algorithms to help filter down results.

Because IMR maintains the same relative error as the original m/z axis, clustering parameters based on expected error (i.e. $x \text{ Da} + y \text{ ppm}$) can be much easier to determine for effective clustering than KMD. Shown below, cluster analysis using DBSCAN algorithms was run on each respectively transformed axis. IMR gives clustered polymer groupings when scaled on the RU basis, given similar setting to binning and align in other applications error = 0.005 Da + 10 ppm. When applied to KMD, the masses overlap much more and in this case cluster parameters had to be determined through trial and error.



Multiple repeat units, charge states, or a combination of the two exist can within a given analysis, making it incredibly difficult to decipher. In these cases, application of IMR with circular distance metrics for rapid assignment becomes extremely valuable. The use of multiple IMR transformations for distinct processing pipelines for each charge state / repeat unit or a single IMR vector used to compute polymetric species can be done in these cases. The distance metric for the vector approach can be more complex, thus the pipelined approach can be more effective and easily interpreted.

Either way, when $z \geq 1$, the additional analysis $n = z$ should be done with for any charge states expected. When applying IMR algorithms, species are detectable if they are spaced by the mass of the repeat unit divided by the RU / n apart. This will limit some of the inefficiencies shown above. The data processing of multiple repeat units and charge states do not add very much to analysis time due to the efficiency of cluster algorithms such as DBscan. The multiple processing pipelines can be implemented effectively through custom Python scripting.

